Available online at www.sciencedirect.com
ScienceDirect
Journal of Solid State Chemistry 180 (2007) 1566–1574
JOURNAL OF SOLID STATE CHEMISTRY
www.elsevier.com/locate/jssc

Synthesis and crystal structure of the palladium oxides $NaPd_3O_4$, Na_2PdO_3 and $K_3Pd_2O_4$

Rodion V. Panin[a,*], Nellie R. Khasanova[a], Artem M. Abakumov[a], Evgeny V. Antipov[a], Gustaaf Van Tendeloo[b], Walter Schnelle[c]

[a]*Department of Chemistry, Moscow State University, 119992, Moscow, Russia*
[b]*EMAT University of Antwerp (RUCA), Groenenborgerlaan 171, B-2020 Antwerp, Belgium*
[c]*Max-Planck Institute for Chemical Physics of Solids, Nöthnitzer Street 40, 01187 Dresden, Germany*

Received 10 January 2007; received in revised form 27 February 2007; accepted 2 March 2007
Available online 12 March 2007

Abstract

$NaPd_3O_4$, Na_2PdO_3 and $K_3Pd_2O_4$ have been prepared by solid-state reaction of Na_2O_2 or KO_2 and PdO in sealed silica tubes. Crystal structures of the synthesized phases were refined by the Rietveld method from X-ray powder diffraction data. $NaPd_3O_4$ (space group $Pm\bar{3}n$, $a = 5.64979(6)$ Å, $Z = 2$) is isostructural to $NaPt_3O_4$. It consists of NaO_8 cubes and PdO_4 squares, corner linked into a three-dimensional framework where the planes of neighboring PdO_4 squares are perpendicular to each other. Na_2PdO_3 (space group $C2/c$, $a = 5.3857(1)$ Å, $b = 9.3297(1)$ Å, $c = 10.8136(2)$ Å, $\beta = 99.437(2)^\circ$, $Z = 8$) belongs to the Li_2RuO_3-structure type, being the layered variant of the NaCl structure, where the layers of octahedral interstices filled with Na^+ and Pd^{4+} cations alternate with Na_3 layers along the c-axis. Na_2PdO_3 exhibits a stacking disorder, detected by electron diffraction and Rietveld refinement. $K_3Pd_2O_4$, prepared for the first time, crystallizes in the orthorhombic space group $Cmcm$ ($a = 6.1751(6)$ Å, $b = 9.1772(12)$ Å, $c = 11.3402(12)$ Å, $Z = 4$). Its structure is composed of planar PdO_4 units connected via common edges to form parallel staggered PdO_2 strips, where potassium atoms are located between them. Magnetic susceptibility measurements of $K_3Pd_2O_4$ reveal a Curie–Weiss behavior in the temperature range above 80 K.

Keywords: Sodium palladium oxide; Potassium palladium oxide; Crystal structure; Electron diffraction; Magnetic susceptibility

1. Introduction

Complex oxides, containing palladium in either the +2 or +4 oxidation state, are not numerous. The oxidation state of palladium in these compounds strongly depends on the synthesis technique. While compounds of divalent palladium, such as Ba_2PdO_3 [1], MPd_3O_4 (M = Ca, Sr, Cd) [2,3] and $Lu_{0.5}Na_{0.5}Pd_3O_4$ [4] have been prepared by a conventional solid-state reaction or hydroxide flux method, a high-pressure technique was applied to synthesize complex oxides containing Pd in higher oxidation states, such as $LnPd_2O_4$ (Ln = La, Pr, Nd, Gd, Y) [5], $LaPdO_3$ [6], Zn_2PdO_4 [7] and M_4PdO_6 (M = Ca, Sr) [8].

It has been reported that palladium is readily oxidized in the presence of alkali metals [9,10]. Nevertheless, the A–Pd–O (A = alkali metal) systems remain unexplored. Only $Na_2Pd_3O_4$ was thoroughly characterized in the Na–Pd–O system [11], whereas $Na_xPd_3O_4$ and Na_2PdO_3, containing highly oxidized Pd, were just briefly described [9,10]. In the K–Pd–O system, besides K_2PdO_2, which is isostructural to K_2PtS_2 [12], the synthesis of K_6PdO_4 and K_2PdO_3 has been reported [10]. For the last two phases only cell parameters without any structure information were given. Moreover, paramagnetic behavior, reported for K_2PdO_3, assumes the presence of mixed-valent palladium, which is in disagreement with the given chemical formula. In order to explore the chemistry of palladium oxides, an investigation of several A–Pd–O systems (A = Na, K) has been undertaken, and complex oxides $NaPd_3O_4$, Na_2PdO_3 and $K_3Pd_2O_4$ have been synthesized and structurally characterized. The different structures of these compounds are discussed in terms of coordination environment of palladium in different oxidation states.

*Corresponding author. Fax: +7 495 939 47 88.
E-mail address: panin@icr.chem.msu.ru (R.V. Panin).

0022-4596/$ - see front matter © 2007 Elsevier Inc. All rights reserved.
doi:10.1016/j.jssc.2007.03.005

2. Experimental

Na_2O_2 (Aldrich, 97%), KO_2 (Aldrich, 95%) and PdO were taken as starting materials. PdO was obtained by dissolving Pd (99.99%) in a mixture of HCl and HNO_3 followed by adding the appropriate amount of $NaNO_3$. The reaction mixture was evaporated and then gradually heated at 350–370 °C and 590–600 °C. The product was carefully washed with water and dried under vacuum. The purity of the prepared PdO was checked by X-ray powder diffraction.

All subsequent operations were carried out in a glove box (MB 120 B-G, MBraun) filled with purified Ar. Mixtures of reagents were intimately ground, pressed into pellets and placed in a corundum crucible. Syntheses were carried out in silica tubes ($V \sim 20\,cm^3$) which were evacuated, then filled with oxygen up to the required pressure and sealed. In all cases, a furnace cooling regime was applied after annealing.

Phase composition and lattice parameters of the compounds were determined by X-ray powder diffraction using a Huber G670 image plate Guinier camera (transmission mode, Cu$K_{\alpha 1}$ radiation). X-ray powder diffraction data for structure refinement were collected with a STOE STADI-P diffractometer (Cu$K_{\alpha 1}$ radiation, linear PSD detector). Structure refinement was carried out by the Rietveld method using the JANA 2000 program [13].

Energy-dispersive X-ray (EDX) analysis was performed with a scanning electron microscope Supra 50VP (LEO Carl Zeiss, Germany) with INCA Energy+ (Oxford, England) spectrometer. The intensities of the Na *K*- and Pd *L*-lines were used to determine the cation composition. Electron diffraction (ED) patterns were obtained using a Philips CM20 transmission electron microscope.

Magnetization measurements of $K_3Pd_2O_4$ were performed on a Quantum Design MPMS-XL7 SQUID magnetometer in the temperature range 1.8–400 K for magnetic fields between 20 Oe and 70 kOe. The sample was handled in an inert atmosphere, for the measurement it was encapsulated in a quartz ampoule pre-calibrated under He gas. A weak field dependence of the magnetic susceptibility was supposed to be due to a minor ferromagnetic impurity of unknown origin. Its amount, corresponded to 50 ppm Fe or an equivalent amount of iron oxides, was on a much lower level to be detected by X-ray diffraction. The high-field data of $\chi(T)$ were corrected for ferromagnetic impurity by the Honda-Owen extrapolation method [14].

3. Results

3.1. Synthesis

Initial amounts of reagents, partial oxygen pressure, time and temperature of annealing were optimized to produce pure $NaPd_3O_4$, Na_2PdO_3 and $K_3Pd_2O_4$ phases. In all cases, some excess of Na_2O_2 or KO_2 was used to compensate for the loss of alkali metal due to volatilization. A single-phase sample of $NaPd_3O_4$ was prepared by heating the mixture of Na_2O_2 and PdO in a molar ratio of 1:4 at 650 °C for 20 h. The starting oxygen pressure in the ampoule was about 0.5 atm. The XRD pattern of the obtained dark powder was indexed on a cubic lattice with the parameter $a = 5.64979(6)$ Å that agrees well with that reported before [9].

Higher temperatures and higher oxygen pressures were applied to synthesize the Na_2PdO_3 phase. Carmine-red Na_2PdO_3 was prepared by annealing a mixture of Na_2O_2 and PdO in a molar ratio of 1.5:1 at 700 °C for 48 h with a starting O_2 pressure of 0.7 atm. The XRD pattern of Na_2PdO_3 was indexed on a monoclinic lattice with unit cell parameters $a = 5.3857(1)$ Å, $b = 9.3297(1)$ Å, $c = 10.8136(2)$ Å, $\beta = 99.437(2)^\circ$. These data are in a good agreement with those previously reported by Wilhelm and Hoppe [10]. The Na:Pd cation ratio determined by EDX analysis of a fresh sample was found to be equal to 64.6(9):35.4(7), close to the nominal 2:1 value.

$K_3Pd_2O_4$ was synthesized from a mixture of KO_2 and PdO in a molar ratio of 2:1 by a two-step annealing: at 600 °C for 20 h, then at 650 °C for 20 h. The starting oxygen pressure in the ampoule was about 0.5 atm. The XRD pattern of the obtained dark-grey powder was indexed on a *C*-centered orthorhombic lattice with unit cell parameters $a = 6.1751(6)$ Å, $b = 9.1772(12)$ Å, $c = 11.3402(12)$ Å. Nevertheless, three weak peaks on the diffraction data remained unidentified, later on they were excluded from the Rietveld refinement.

Na_2PdO_3 and $K_3Pd_2O_4$ were found to be very sensitive to moisture and for X-ray diffraction studies they were sealed into glass capillaries of 0.2 mm diameter.

3.2. Structure of $NaPd_3O_4$

The structure of $NaPd_3O_4$ was refined in the $Pm\bar{3}n$ space group with the atomic coordinates of $NaPt_3O_4$ as starting values [15]. Isotropic atomic displacement parameters (ADPs) were applied for all atoms. The refinement of the Na site occupation factor provided a value of 1.03(1) and confirmed thereby full occupation of this position. No improvement was achieved by symmetry lowering from $Pm\bar{3}n$ to $P\bar{4}3n$, that resulted in a shift of the *O*-position from (1/4,1/4,1/4) to (*x*,*x*,*x*) (as in $Li_{0.64}Pt_3O_4$ [16]). The deviation from $x = 1/4$ was negligible. The refinement in the $Pm\bar{3}n$ space group provided reasonable structural parameters and a good fit of the experimental data (Fig. 1). Crystallographic parameters of $NaPd_3O_4$ and details on the structure determination are given in Table 1, atomic coordinates and isotropic ADPs in Table 2.

The structure of $NaPd_3O_4$ consists of NaO_8 cubes and PdO_4 squares. The latter are linked by their corners and form a three-dimensional framework where the planes of neighboring PdO_4 squares are perpendicular to each other (Fig. 2).

3.3. Structure of Na_2PdO_3

Only reflections with $h + k = 2n$ were observed on the XRD pattern of Na_2PdO_3, indicating a *C*-centered unit

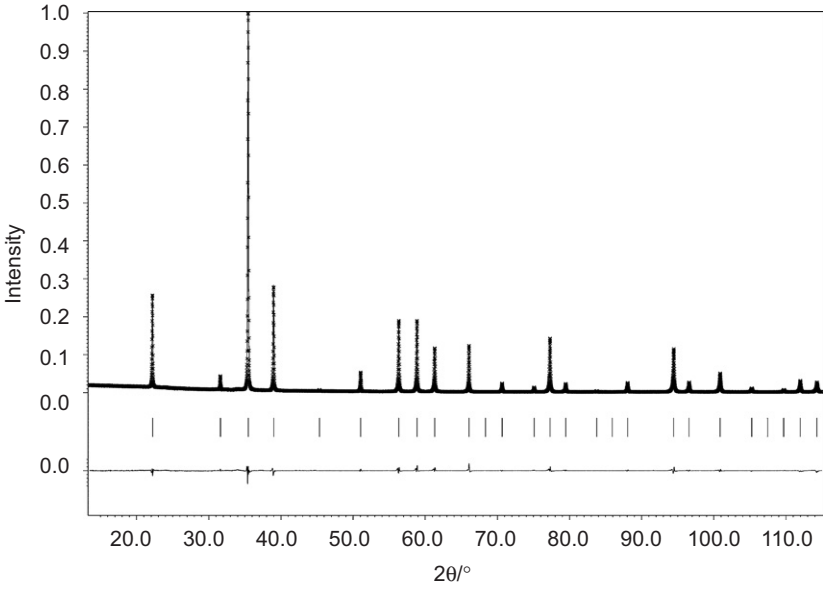

Fig. 1. XRD profile after Rietveld refinement for $NaPd_3O_4$: observed (cross), calculated (full line), and difference (bottom) profiles. Tick markers indicate the Bragg reflection position.

Table 1
Crystallographic data and details on the structure determination of $NaPd_3O_4$

Crystallographic data	
Crystal system	Cubic
Space group	$Pm\bar{3}n$ (no. 223)
Cell constant a (Å)	5.64979(6)
Cell volume V (Å^3)	180.342(3)
Formula units Z	2
Molecular weight	406.19
Calculated density (g/cm^3)	7.449
Data collection and structure refinement	
Radiation and wavelength	Cu$K_{\alpha1}$, $\lambda = 1.5406$ Å
Temperature (K)	295
2θ range (deg.)	13.5–115
Number of measured reflections	32
No. of refined parameters	14
Reliability factors	$R_I = 0.022$, $R_{wp} = 0.064$, $R_p = 0.043$, GOF = 1.37

Table 2
Atomic coordinates and isotropic displacement parameters of $NaPd_3O_4$

Atom	Position	x/a	y/b	z/c	U_{iso} (Å^2)
Na	2*a*	0	0	0	0.0187(6)
Pd	6*c*	0.25	0	0.5	0.0134(1)
O	8*e*	0.25	0.25	0.25	0.0154(6)

cell. To determine the space group for Na_2PdO_3, an ED study was performed. All intense reflections on the ED patterns (Fig. 3) can be indexed on the base of a monoclinic unit cell with $a\sim5.35$ °Å, $b\sim9.29$ °Å, $c\sim10.76$ °Å, $\beta\sim99.2°$. The reflection condition *h0l*: h, $l = 2n$ observed on the [010]* pattern is in agreement with the possible space groups *Cc* and *C*2/*c*. ED patterns of [100]*, [001]* and [301]* zones satisfy both space groups. Apart from the intense reflections, additional diffuse streaks have been detected on the [100]* pattern. To build the initial model, derivatives of the NaCl-structure type with the A_2BO_3 formula were analyzed. Three structure models, Li_2SnO_3 [17], Li_2MnO_3 [18] and Li_2RuO_3 [19], are known with *C*2/*c* symmetry. These structures can be considered as derivatives of the NaCl type with the following transformation matrix:

$$\begin{pmatrix} \frac{1}{2} & \frac{1}{2} & 1 \\ -\frac{3}{2} & \frac{3}{2} & 0 \\ -\frac{4}{3} & -\frac{4}{3} & \frac{4}{3} \end{pmatrix}.$$

The unit cells of Na_2PdO_3 and NaCl are related as follows: $a\sim\sqrt{3/2}\,a_{NaCl}$, $b\sim3/\sqrt{2}\,a_{NaCl}$, $c\sim4/\sqrt{3}\,a_{NaCl}$. The oxygen atoms in these structures form a cubic close packing where octahedral voids are occupied by metal atoms. Ordering of A and B cations takes place along the [111] direction of the cubic NaCl which defines the *c*-axis of the monoclinic crystal system. It leads to the formation of layers with interstices filled with only A^+ cations (A_3 layers) and with both A^+ and B^{4+} cations in a 1:2 ratio (AB_2O_6 slabs). These two fragments stack in an alternating mode along the *c*-axis (Fig. 4). Different structure models are distinguished by the relative arrangement of the AB_2O_6 slabs. In Li_2MnO_3 and Li_2RuO_3, the AB_2O_6 slabs, separated by $c/2$, are shifted by $\left[\frac{1}{2}00\right]$ (Fig. 5a), while in Li_2SnO_3 the displacement vector is equal to $\left[0\frac{1}{6}0\right]$ (Fig. 5b). These translations are the intrinsic translations relating the A_3 layers at z and $z+\frac{1}{2}$ in both structure types (Fig. 5c). The Li_2RuO_3 and Li_2MnO_3 types are discerned by the existence of one or two crystallographically independent B atom positions within the AB_2O_6 slab, respectively, because of an origin shift by $\left[00\frac{1}{4}\right]$. For Li_2MnO_3, another modification

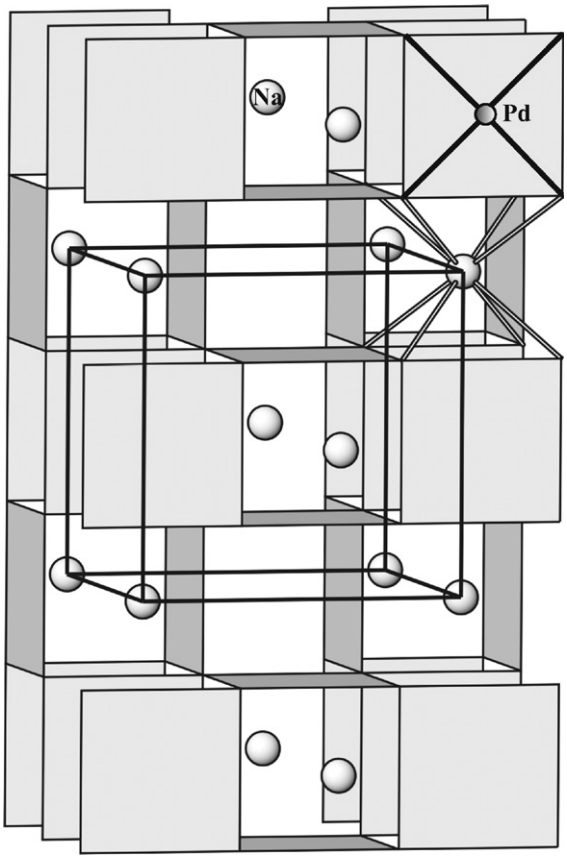

Fig. 2. Crystal structure of $NaPd_3O_4$. PdO_4 squares and Na cations are drawn.

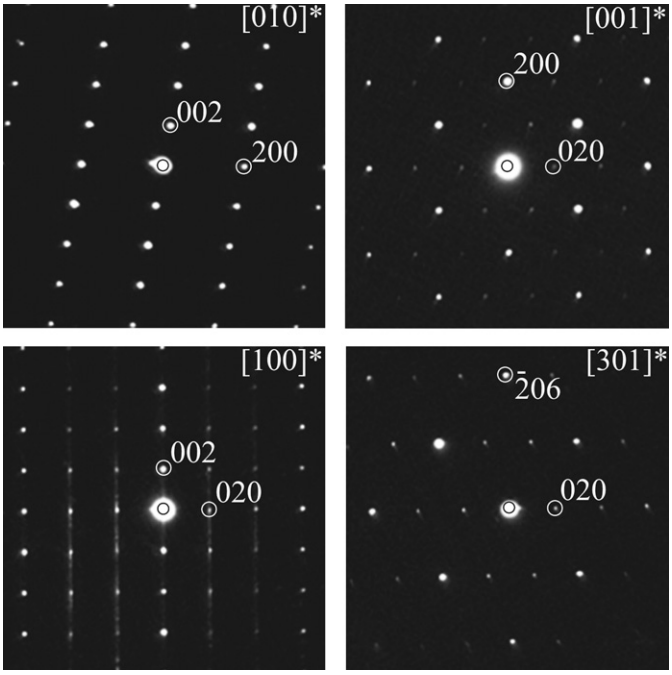

Fig. 3. Electron diffraction patterns of Na_2PdO_3 along the main zone axes.

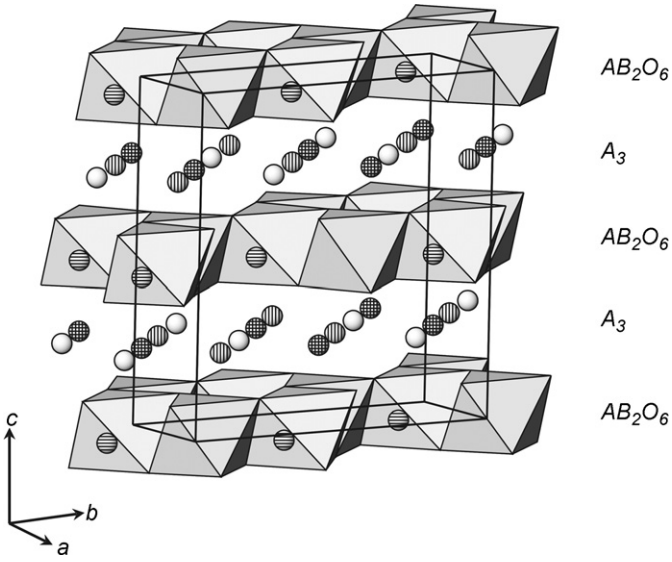

Fig. 4. Alternation of AB_2O_6 slabs and A_3 layers in the structure of A_2BO_3. BO_6 octahedra and A-cations are drawn.

with a halved c-parameter, where the AB_2O_6 slab shift is absent, was also described [20]. However, it does not match with the observed ED and X-ray patterns of Na_2PdO_3 and therefore it was not considered.

An appropriate structure model was selected on the base of ED pattern simulation. While calculated ED patterns of the [010]* and [301]* zones were identical for all models, the [100]* pattern (without diffuse streaking) was in a good agreement with the Li_2MnO_3 and Li_2RuO_3 types: only for these models reflections $0\,k\,l$ with $l = 2n+1$ have zero intensity. Based on these findings a model with a layer stacking similar to the one in Li_2MnO_3 and Li_2RuO_3 was chosen. Nevertheless, the diffuse streaking along c^*, observed on the [100]* ED pattern, indicates the presence of some stacking disorder. It should be noticed that unstreaked spots on the [100]* zone are observed only for $0\,k\,l$ with $k = 6n$. From this condition for the occurrence of unstreaked spots, using the $\mathbf{g}\cdot\mathbf{R} = \text{integer}$ criterium, (where $\mathbf{g}$ is the diffraction vector) one can deduce a displacement vector $\mathbf{R} = \left[u\tfrac{1}{6}0\right]$ for the defect planes, responsible for the diffuse streaking along the c^*-axis [21]. The $u = \frac{1}{2}$ requirement is derived from Rietveld refinement later on. Random stacking of the AB_2O_6 slabs shifted either over $\left[\tfrac{1}{2}0\,0\right]$ or over $\left[\tfrac{1}{2}\tfrac{1}{6}0\right]$ causes the appearance of diffuse intensity along c^*. Being layered variants of the NaCl-type, Li_2SnO_3, Li_2MnO_3 and Li_2RuO_3 are closely related, and this similarity leads to stacking disorder and to the observation of diffuse intensity streaks on the ED pattern of Na_2PdO_3.

Rietveld refinement was performed in the $C2/c$ space group using the Li_2RuO_3 and Li_2MnO_3 structure data. In the initial stages, constrains were imposed on the Pd(1)–O and Na(1)–O distances (2.00 ± 0.05 Å and 2.30 ± 0.05 Å, respectively). Isotropic ADPs of Na_2PdO_3 were constrained to be equal for each type of atom. Refinement using the Li_2RuO_3 structure model leads to the following

reliability factors: $R_{wp} = 0.098$, $R_p = 0.071$, $R_I = 0.101$. As a next step, ADP of the Na(1) site was refined independently. It considerably decreased the R-factors ($R_{wp} = 0.079$, $R_p = 0.061$, $R_I = 0.069$), and the values $U_{Pd(1)} = 0.053\,Å^2$ and $U_{Na(1)} = -0.004\,Å^2$ were obtained. We assumed that these values result from the partial occupation of the Na(1) site by Pd atoms and the Pd(1) site by Na atoms. Such mixed occupation of cation sites within the $NaPd_2O_6$ slab results from the stacking disorder introduced by the displacement vector $\mathbf{R}\ \left[\frac{1}{2}\frac{1}{6}0\right]$. The $u = \frac{1}{2}$ component is necessary to exchange the Na and Pd positions within the layer. Refinement of the occupancy factors proved the presence of about 12% Na on the Pd(1) site. A similar procedure carried out for the Na(1) position led to a Na/Pd ratio of 0.716(8)/0.284(8). This is in reasonable agreement with refinement results for the Pd(1) site considering the position multiplicities. Taking into account these findings and the results of the EDX analysis (see Section 3.1) we assumed that the Na amount on the Pd(1) site is equal to the Pd amount on the Na(1) site. Final refinement with these constraints resulted in reasonable R-factor values ($R_{wp} = 0.060$, $R_p = 0.046$, $R_I = 0.055$) and a good fit with the experimental data (Fig. 6). Refinement using the Li_2MnO_3 model (with two independent Pd positions) did not improve the fit ($R_{wp} = 0.062$, $R_p = 0.047$, $R_I = 0.057$), and therefore the Li_2RuO_3 model was chosen. Final experimental and crystallographic parameters refined in the Li_2RuO_3 model are given in Table 3. Atomic parameters and selected bond lengths are shown in Tables 4 and 5.

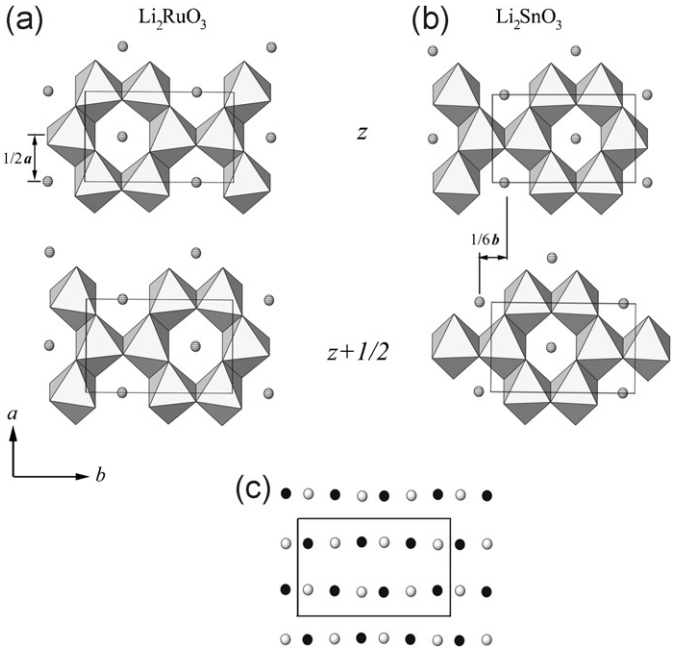

Fig. 5. Projection of the neighboring AB_2O_6 slabs on the a–b plane at z and $z+1/2$: (a) Li_2RuO_3; (b) Li_2SnO_3 and (c) projection of two neighboring Na_3 layers on the same plane, white and black circles correspond to atoms shifted by $c/2$ layers.

All cations in the Na_2PdO_3 structure are coordinated octahedrally. The Pd–O distances (1.98–2.08 Å) are in a good agreement with previously reported data for Pd^{4+}. For the Na(2)–Na(4) sites, the Na–O distances are in the range of 2.23–2.67 Å, while the Na(1)–O distances are shorter: 2.23–2.24 Å.

3.4. Structure and properties of $K_3Pd_2O_4$

Only reflections with $h+k = 2n$ were observed on the XRD pattern of $K_3Pd_2O_4$, indicating a C-centered unit cell. Further analysis of the XRD pattern revealed the following

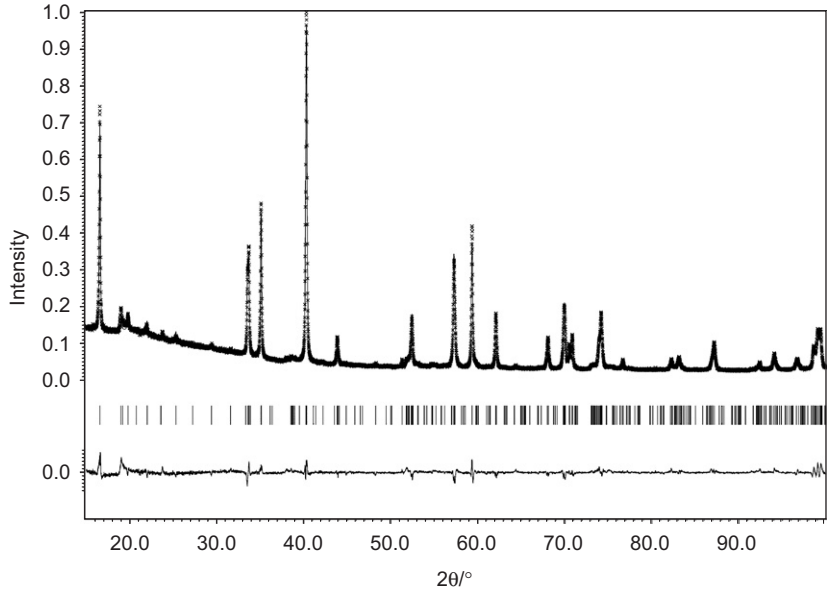

Fig. 6. XRD profile after Rietveld refinement for Na_2PdO_3: observed (cross), calculated (full line), and difference (bottom) profiles. Tick markers indicate the Bragg reflection positions.

Table 3
Crystallographic data and details on the structure determination of Na_2PdO_3

Crystallographic data	
Crystal system	Monoclinic
Space group	$C2/c$ (no. 15)
Cell parameters	
a (Å)	5.3857(1)
b (Å)	9.3297(1)
c (Å)	10.8136(2)
β (deg.)	99.437(2)
Formula units Z	8
Molecular weight	200.38
Cell volume V (Å^3)	536.00(2)
Calculated density (g/cm^3)	4.966
Data collection and structure refinement	
Radiation and wavelength	Cu$K_{\alpha1}$, $\lambda = 1.5406$ Å
Temperature (K)	295
2θ range (deg.)	15–98
No. of measured reflections	118
No. of refined parameters	24
Reliability factors	$R_I = 0.055$, $R_p = 0.046$, $R_{wp} = 0.060$, GOF = 1.88

Table 4
Atomic positions and displacement parameters of Na_2PdO_3

Atom	Position	x/a	y/b	z/c	U_{iso} (Å^2)
Pd(1)[a]	8*f*	0.2601(5)	0.0829(2)	−0.0006(4)	0.0308(7)
Na(1)[b]	4*c*	0.75	0.25	0.0	0.0263(5)
Na(2)	4*e*	0.5	0.5792(11)	0.25	0.0263(5)
Na(3)	4*e*	0.0	0.4159(13)	0.25	0.0263(5)
Na(4)	4*c*	0.0	0.75	0.25	0.0263(5)
O(1)	8*f*	0.3505(10)	0.2504(11)	−0.1002((8)	0.0235(8)
O(2)	8*f*	0.5980(14)	0.0709(14)	0.1053(13)	0.0235(8)
O(3)	8*f*	0.593(2)	0.4299(14)	0.1013(13)	0.0235(8)

[a]Occupancy 0.874(7) Pd + 0.126(7) Na.
[b]Occupancy 0.748(7) Na + 0.252(7) Pd.

additional reflection conditions *h 0 l*: h, $l = 2n$; *0 0 l*: $l = 2n$; in agreement with the space groups $Cmc2_1$ and *Cmcm*. Since the XRD pattern of $K_3Pd_2O_4$ resembles the $K_3Pt_2O_4$ diffraction data, these compounds were proposed to be isostructural. Therefore, the Rietveld refinement was started in the *Cmcm* space group with the atomic coordinates of $K_3Pt_2O_4$ as the starting values [22]. Isotropic ADPs were applied for all atoms. The refinement of the *K* site occupation factors resulted in values of 0.997(4) for the *K*(1) and 1.004(5) for the *K*(2) confirming a full occupation of these positions. Structure refinement carried out in this way provided reasonable *R*-factors ($R_{wp} = 0.045$, $R_p = 0.0341$, $R_I = 0.0274$) and an acceptable fit of the experimental data (Fig. 7). Crystallographic parameters of $K_3Pd_2O_4$ and details on the structure refinement are given in Table 6, atomic coordinates and isotropic ADPs in Table 7 and the selected interatomic distances in Table 8.

In the $K_3Pd_2O_4$ structure, Pd atoms are coordinated by four oxygen atoms in a rectangular–planar arrangement.

Table 5
Selected interatomic distances for Na_2PdO_3

Bond	d (Å)	Bond	d (Å)
Pd(1)–O(1)	1.993(10)	Na(2)–O(1)	2 × 2.482(11)
Pd(1)–O(1)	2.033(10)	Na(2)–O(2)	2 × 2.444(9)
Pd(1)–O(2)	1.979(9)	Na(2)–O(3)	2 × 2.234(15)
Pd(1)–O(2)	2.041(14)	Na(3)–O(1)	2 × 2.458(14)
Pd(1)–O(3)	2.024(13)	Na(3)–O(2)	2 × 2.245(15)
Pd(1)–O(3)	2.082(15)	Na(3)–O(3)	2 × 2.489(13)
Na(1)–O(1)	2 × 2.232(7)	Na(4)–O(1)	2 × 2.267(8)
Na(1)–O(2)	2 × 2.238(14)	Na(4)–O(2)	2 × 2.395(14)
Na(1)–O(3)	2 × 2.232(14)	Na(4)–O(3)	2 × 2.421(14)

The PdO_4 units share common edges to form parallel staggered corrugated strips running along the *c*-axis, and the potassium atoms are located between the strips (Fig. 8). There are two independent Pd positions alternating within each PdO_2 strip, the Pd–O distances for both Pd(1) and Pd(2) sites were refined to be equal to 2.001 Å. Bond valence sum (BVS) calculation with the r_0 constant of Pd^{2+} yields the value of 2.27 that is apparently underestimated comparing to the chemical formula. The *K*(1) atom is coordinated by six oxygen atoms in a slightly distorted trigonal prism with *K*(1)–O bonds of 2.763–2.917 Å (Fig. 8b). The *K*(2) atom has an unusual asymmetric coordination: it is coordinated by four oxygen atoms with a *K*(2)–O bond of 2.647 Å. Due to a repulsion between the *K*(2) and the Pd(2) atoms the other four oxygen atoms are shifted away by 3.878 Å, therefore these interactions are hardly to be considered as bonding ones. A BVS calculation for *K*(2), considering nearest oxygen atoms, provides a value of 1.0. Furthermore the same coordination behavior of the *K*(2) atom is observed in $K_3Pt_2O_4$ and $K_3Ni_2O_4$, which are isostructural with $K_3Pd_2O_4$.

The temperature dependence of $1/\chi$ for the $K_3Pd_2O_4$ sample is presented in Fig. 9. For high fields it roughly displays a Curie–Weiss law. After correction for diamagnetic core contribution ($\chi_{dia} = -137 \times 10^{-6}$ emu mol^{-1}), a good fit with a Curie–Weiss law with $\theta = -80$ K in the temperature range 80–400 K is obtained. The effective magnetic moment μ_{eff} per f.u. is found to be 1.80 μ_B. Considering formally the ionic limit, this experimental value would be compatible with the sum of the spin only moments calculated for one Pd^{2+} (no unpaired electron for the square-planar coordination) and one Pd^{3+} (one unpaired electron for this coordination, giving 1.73 μ_B), i.e. an average Pd(+2.5). Deviations from the Curie–Weiss law are observed below 60 K. A weak maximum of $\chi(T)$ at around 50 K might be eventually due to a contamination with (strongly paramagnetic) solid molecular γ-oxygen. The value of the Weiss parameter θ signals relatively strong antiferromagnetic interactions of the transition metal species; however, no signs of a bulk phase transition is found above 1.8 K. The impurity found by XRD is supposed to be diamagnetic or paramagnetic one, in the last case, the correction to the paramagnetic moment would be quite insignificant (less than 0.1 μ_B).

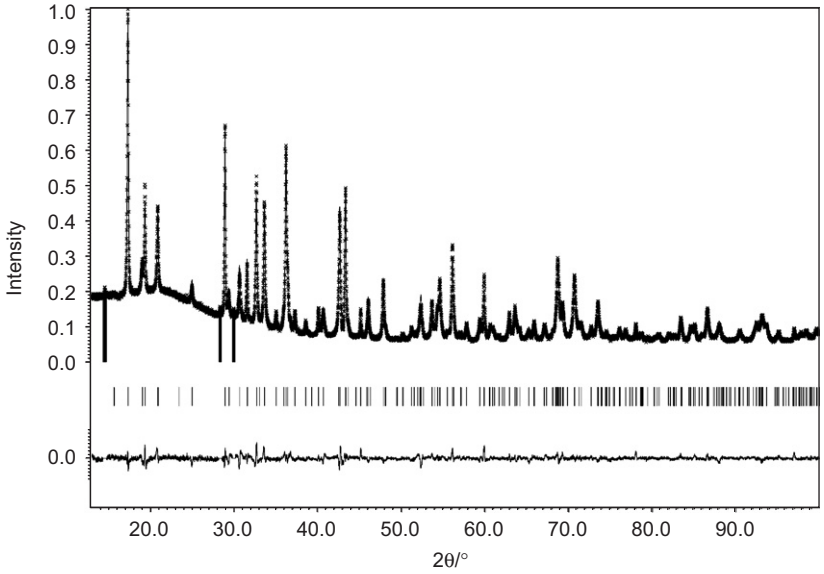

Fig. 7. XRD profile after Rietveld refinement for $K_3Pd_2O_4$: observed (cross), calculated (full line), and difference (bottom) profiles. Tick markers indicate the Bragg reflection positions.

Table 6
Crystallographic data and details on the structure determination of $K_3Pd_2O_4$

Crystallographic data	
Crystal system	Orthorhombic
Space group	*Cmcm* (no. 63)
Cell parameters	
a (Å)	6.1751(6)
b (Å)	9.1772(12)
c (Å)	11.3402(12)
Formula units *Z*	4
Molecular weight	394.06
Cell volume *V* (Å^3)	642.65(12)
Calculated density (g/cm^3)	4.0719
Data collection and structure refinement	
Radiation and wavelength	Cu$K_{\alpha1}$, $\lambda = 1.5406$ Å
Temperature (K)	295
2θ range (deg.)	13–100
No. of measured reflections	105
No. of refined parameters	38
Reliability factors	$R_I = 0.0274$, $R_p = 0.0341$, $R_{wp} = 0.045$, GOF = 1.56

Table 7
Atomic positions and displacement parameters of $K_3Pd_2O_4$

Atom	Position	*x*/*a*	*y*/*b*	*z*/*c*	U_{iso} (Å^2)
Pd(1)	4*a*	0	0	0	0.0103(4)
Pd(2)	4*c*	0	0.0735(1)	0.25	0.0091(5)
K(1)	8*f*	0	0.3543(2)	0.0681(2)	0.0190(7)
K(2)	4*c*	0	0.7153(3)	0.25	0.0153(10)
O(1)	16*h*	0.2867(5)	0.4227(5)	0.8829(4)	0.0080(13)

The magnetic behavior of $K_3Pd_2O_4$ is similar to its Ni and Pt analogs [22]: the temperature dependence of $\chi(T)$ could be approximated by a Curie–Weiss law down to ca. 50 K. The effective magnetic moments (calculated in the same manner as above) of the compounds are however different ($K_3Pt_2O_4$: 1.39 μ_B/f.u., $K_3Ni_2O_4$: 2.53 μ_B/f.u., respectively). The different μ_{eff} values may be rationalized by the well-known different spin–orbital and ligand–field interactions of the 3*d*, 4*d* and 5*d* elements. Actually, the magnetic moment of $K_3Pd_2O_4$ fits in between the values of the lighter and heavier analogs.

Table 8
Selected interatomic distances for $K_3Pd_2O_4$

Bond	*d* (Å)
Pd(1)–O(1)	4 × 2.001(4)
Pd(2)–O(1)	4 × 2.001(4)
Pd(1)–Pd(2)	2 × 2.9142(3)
K(1)–O(1)	2 × 2.763(4)
K(1)–O(1)	2 × 2.818(4)
K(1)–O(1)	2 × 2.917(5)
K(2)–O(1)	4 × 2.647(4)

4. Discussion

As already mentioned, compounds containing Pd in an oxidation state higher than +2 are sparse and usually prepared under elevated oxygen pressure. Upon palladium oxidation (from +2 to +4) its coordination polyhedron transforms from planar PdO_4 to octahedral PdO_6. This is explained by a change of electron configuration: the ligand field stabilization energy of the d^8 configuration causing the square planar coordination of Pd^{2+} vanishes upon removal of electrons, and for Pd^{3+} (d^7) and Pd^{4+} (d^6) the octahedral coordination becomes preferable, as it occurs respectively in $LaPdO_3$ [6] and the inverse spinel Zn_2PdO_4 [7].

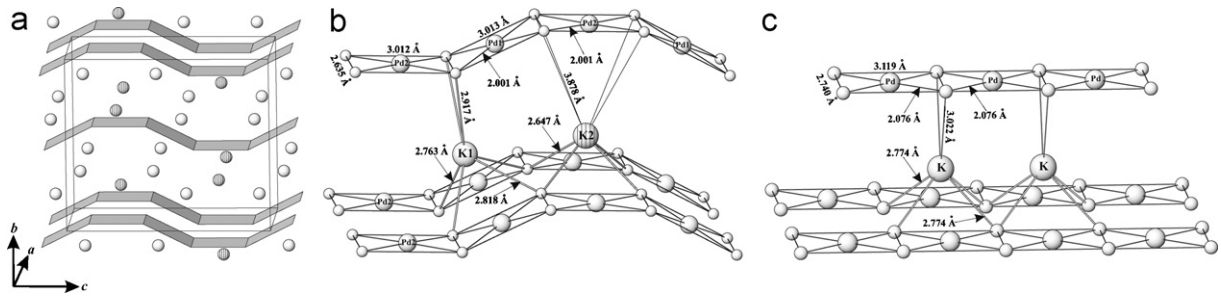

Fig. 8. (a) Crystal structure of $K_3Pd_2O_4$: staggered PdO_2 strips formed by PdO_4 units and *K* atoms between them are drawn; (b) coordination environment of Pd and *K* atoms in the $K_3Pd_2O_4$ structure; (c) coordination environment of Pd and *K* atoms in the structure of K_2PdO_2.

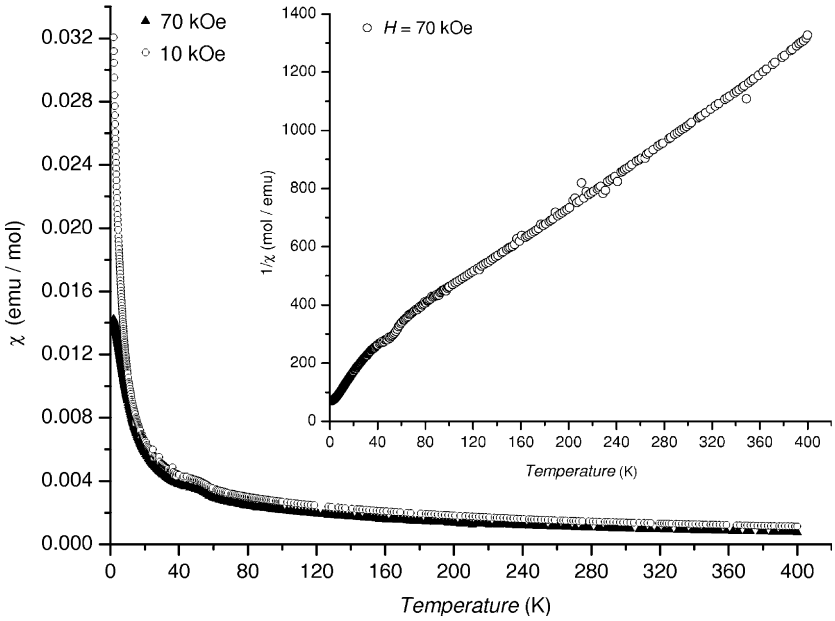

Fig. 9. Temperature dependence of the inverse magnetic susceptibility $1/\chi(T)$ and of $\chi(T)$ (inset) of the $K_3Pd_2O_4$ sample.

The square planar coordination of palladium remains preferable in the mixed valent palladates. Thus, a three-dimensional network of $NaPd_3O_4$, containing Pd in an oxidation state of +2.33, is composed of PdO_4 squares that share common corners. The Pd–O bond (1.999 Å) in this compound is shorter comparing to that of the isostructural phases $CaPd_3O_4$ (2.048 Å), $SrPd_3O_4$ (2.055 Å) [2] and $CdPd_3O_4$ (2.030 Å) [3] containing Pd^{2+}. The B_3O_4 framework (B = Pd or Pt) is quite rigid (Fig. 2); its dimensions, as well as the size of the atoms that can be arranged in a cubic coordination environment, depends on the *B*–O bond length, i.e. on the oxidation state of Pd or Pt. This explains unsuccessful attempts to synthesize similar compound with potassium, the ionic radius of which is about 30% larger than that of sodium ($r(K^+) = 1.38$ Å and $r(Na^+) = 1.02$ Å) [23].

Typical for Pd^{4+}, an octahedral coordination exists in Na_2PdO_3. Its structure is a partially ordered derivative of the NaCl-type. Ordering of Pd^{4+} and Na^+ due to the size difference ($r(Pd^{4+}) = 0.62$ Å and $r(Na^+) = 1.02$ Å [23] in an octahedral coordination) leads to the formation of a layered structure of the Li_2RuO_3-type. The Pd–O bond length defines the dimensions of the PdO_6 octahedra, connected via common edges, and thereby the type of *A*-cations that can order with Pd within the APd_2O_6 slabs. Two positions of the $NaPd_2O_6$ slabs relative to the Na_3 layers, which appear by inducing a $\left[\frac{1}{2}\frac{1}{6}0\right]$ shift, seem to be approximately equal in energy, and this leads to a stacking disorder observed by ED and by the structure refinement. The same feature was recently reported for Na_2RuO_3: in a first approximation its structure was described as a superposition of ordered Li_2SnO_3-type and disordered α-$NaFeO_2$-type [24]. Interestingly, the Na_2PtO_3 phase crystallizes in the Li_2SnO_3-type rather than in the Li_2RuO_3-type, despite close ionic radii of Pd^{4+} and Pt^{4+}. Two other modifications of Na_2PtO_3 can be obtained by direct interaction of Na_2O_2 with Pt and by decomposition of $Na_2[Pt(OH)_6$: β-$Na_2PtO_3]$ is composed of a three-dimensional network of edge-linked PtO_6 octahedra, while the γ-modification crystallizes in the NaCl-type with completely disordered Na and Pd atoms [25,26]. However, we did not observe their Pd analogs in our experiments.

The structure of complex palladium oxides is not only determined by the oxidation state of palladium, but is also

forced by the other constituent atoms. An increase of the *A*-cation size supports the common tendency to form structures with low-dimensional fragments. The structure of $K_3Pd_2O_4$ containing Pd in an oxidation state of +2.5 is built up from staggered strips of edge-sharing PdO_4 groups with potassium atoms located between them. The ideal square planar arrangement of PdO_4 units is considerably distorted: they are stretched along the strip axis and can better be described as rectangles rather than squares. This distortion is typical for one-dimensional structures of palladium oxides and originates from the mutual repulsion between adjacent Pd atoms inside the PdO_2 strips [27]. There are two independent Pd positions in the $K_3Pd_2O_4$ structure; however, the difference between the Pd(1)–O and Pd(2)–O bond lengths is negligible to assume any charge ordering in the structure.

It is interesting to compare the structure of $K_3Pd_2O_4$ with that of K_2PdO_2 built up by straight PdO_2 strips and potassium atoms placed between them. Upon palladium oxidation from +2.0 (K_2PdO_2) to +2.5 ($K_3Pd_2O_4$), the Pd planar rectangular coordination and the type of PdO_4 conjugation are preserved; however, the accommodation of a smaller amount of K atoms results in a $K_3Pd_2O_4$ structure with corrugated staggered PdO_2 strips rather than straight ones (Fig. 8b and c).

No charge ordering is observed in the $LnPd_2O_4$ (Ln = La, Pr, Nd, Gd, Y) structures containing palladium in the same oxidation state. The structure of $LnPd_2O_4$ differs greatly from that of $K_3Pd_2O_4$: its three-dimensional framework is composed of square planar PdO_4 units connected through the common corners. Despite this the coordination environment of Pd atoms in these compounds is similar, furthermore the observed Pd–O distances are quite close (1.996–2.01 Å) that correlates with the identical oxidation state of Pd in these compounds. In contrast to these phases, a charge separation was found in the $Ba_2Hg_3Pd_7O_{14}$ structure having crystallographically distinct sites with square planar and octahedral coordination that are occupied by Pd^{2+} and Pd^{4+}, respectively [28].

Acknowledgments

The work was supported in part by the IAP V-1 program of the Belgium government. Authors are grateful to A.V. Knot′ko and A.V. Garshev (Department of Chemistry, Moscow State University) for EDX analysis and to R.V. Shpanchenko and P.S. Chizhov for their help in X-ray powder data collection for structural refinement.

References

[1] Y. Laligant, A. Le Bail, G. Ferey, M. Hervieu, B. Raveau, A. Wilkinson, A.K. Cheetham, Eur. J. Solid State Inorg. Chem. 25 (1988) 237.
[2] P.L. Smallwood, M.D. Smith, H.-C. Zur Loye, J. Cryst. Growth 216 (2000) 299.
[3] O. Muller, R. Roy, Adv. Chem. Ser. 98 (1971) 28.
[4] S.J. Mugavero III, M.D. Smith, H.-C. Zur Loye, J. Solid State Chem. 179 (2006) 3586.
[5] G. Kramer, E. Hagele, N. Wagner, M. Jansen, Z. Anorg. Allg. Chem. 622 (1996) 1027.
[6] S.-J. Kim, S. Lemaux, G. Demazeau, J.-Y. Kim, J.-H. Choy, J. Am. Chem. Soc. 123 (2001) 10413.
[7] G. Demazeau, I. Omeran, M. Pouchard, P. Hagenmuller, Mater. Res. Bull. 11 (1976) 1449.
[8] Y. Wang, D. Walker, B.-H. Chen, B.A. Scott, J. Alloy Compd. 285 (1999) 98.
[9] J.J. Scheer, A.E. van Arkel, R.D. Heyding, Can. J. Chem. 33 (1955) 683.
[10] Von M. Wilhelm, R. Hoppe, Z. Anorg. Allg. Chem. 424 (1976) 5.
[11] VonM. Wilhelm, R. Hoppe, Z. Anorg. Allg. Chem. 409 (1974) 60.
[12] H. Sabrowsky, W. Bronger, D. Schmitz, Z. Naturforschung, Teil B. Anorganische Chemie, Org. Chem. 29 (1974) 10.
[13] V. Petricek, M. Dusek, JANA2000: Programs for Modulated and Composite Crystals, Institute of Physica, Praha, Czech Republic, 2000.
[14] K. Honda, Ann. Phys. (Leipzig) 32 (1910) 1027.
[15] K.B. Schwartz, C.T. Prewitt, Acta Crystallogr. B 38 (1982) 363.
[16] K.B. Schwartz, J.B. Parise, C.T. Prewitt, R.D. Shannon, Acta Crystallogr. B 38 (1982) 2109.
[17] G. Kreusburg, F. Stewner, R. Hoppe, Z. Anorg. Allg. Chem. 379 (1970) 242.
[18] M. Jansen, R. Hoppe, Z. Anorg. Allg. Chem. 397 (1973) 279.
[19] H. Kobayashi, R. Kanno, Y. Kawamoto, M. Tabuchi, O. Nakamura, M. Tanaka, Solid State Ion. 82 (1995) 25.
[20] P. Strobel, B. Lambert-Andron, J. Solid State Chem. 75 (1988) 90.
[21] D. Van Dyck, R. De Ridder, G. Van Tendeloo, S. Amelinckx, Phys. Stat. Sol. A 43 (1977) 541.
[22] Von H. Zentgraf, K. Claes, R. Hoppe, Z. Anorg. Allg. Chem. 462 (1980) 92.
[23] R.D. Shannon, C.T. Prewitt, Acta Crystallogr. B 25 (1969) 925.
[24] K.M. Mogare, K. Friese, W. Klein, M. Jansen, Z. Anorg. Allg. Chem. 630 (2004) 547.
[25] W. Urland, R. Hoppe, Z. Anorg. Allg. Chem. 392 (1972) 23.
[26] J. Hauck, Z. Naturforschung, Teil B 31 (1976) 1179.
[27] B.L. Dubey, J.A. Gard, F.P. Glasser, A.R. West, J. Solid State Chem. 6 (1973) 329.
[28] T. Hansen, Hk. Muller-Buschbaum, Z. Anorg. Allg. Chem. 616 (1992) 67.